

Age Determination Method of Pre-Main Sequence Stars with High-Resolution *I*-Band Spectroscopy^{*†}

Yuhei TAKAGI, Yoichi ITOH

Graduate School of Science, Kobe University, 1-1 Rokkodai, Nada, Kobe, Hyogo 657-8501

takagi@stu.kobe-u.ac.jp

and

Yumiko OASA

Faculty of Education, Saitama University, 255 Shimo-Okubo, Sakura, Saitama, Saitama 338-8570

(Received ; accepted)

Abstract

We present a new method for determining the age of late-K type pre-main sequence (PMS) stars by deriving their surface gravity from high-resolution *I*-band spectroscopy. Since PMS stars contract as they evolve, age can be estimated from surface gravity. We used the equivalent width ratio (EWR) of nearby absorption lines to create a surface gravity diagnostic of PMS stars that is free of uncertainties due to veiling. The ratios of Fe (8186.7Å and 8204.9Å) and Na (8183.3Å and 8194.8Å) absorption lines were calculated for giants, main-sequence stars, and weak-line T Tauri stars. Effective temperatures were nearly equal across the sample. The Fe to Na EWR (Fe/Na) decreases significantly with increasing surface gravity, denoting that Fe/Na is a desirable diagnostic for deriving the surface gravity of pre-main sequence stars. The surface gravity of PMS stars with $0.8 M_{\odot}$ is able to be determined with an accuracy of 0.1-0.2, which conducts the age of PMS stars within a factor of 1.5, in average.

Key words: stars: evolution — stars: pre-main sequence

1. Introduction

The age of pre-main sequence (PMS) stars is a vital parameter for studying the evolution of young stars. Accurate ages are needed to describe the evolutions of both the photosphere (e.g., rotational processes, chemical evolution) and the circumstellar material (e.g., circumstel-

* Based in part on data collected at Subaru Telescope, which is operated by the National Astronomical Observatory of Japan.

† This research has made use of the SIMBAD database, operated at CDS, Strasbourg, France.

lar disk, protoplanets, outflows). Determining the age of PMS stars lets us study the evolution of the stars themselves and the history of star formation in their star-forming region (e.g., Palla & Stahler 2002). Age is usually determined by comparing the luminosity and the effective temperature (T_{eff}) estimated from broadband photometry or spectroscopy with stellar evolution tracks on the Hertzsprung-Russell (H-R) diagram (Cohen & Kuhi 1979; Strom et al. 1989; Kenyon & Hartmann 1995). However, a precise estimate of PMS star luminosity is difficult. This difficulty arises from extinction, uncertainties in the distance measurements, and continuum excess caused from accretion and the heated circumstellar disk (e.g., veiling). These uncertainties may lead to an incorrect luminosity value.

The age of a PMS star is able to be determined by estimating the surface gravity (g) instead of the luminosity. The surface gravity of a PMS star increases with time because of photospheric contraction. Spectroscopic observations are suitable for determining stellar parameters such as T_{eff} , $\log g$, metal abundance, and radial velocity, since the absorption line profile depends on these parameters. Although the spectra of PMS stars are veiled by the excess, the equivalent width ratio (EWR) of absorption lines is less contaminated by veiling (Meyer et al. 1998). Meyer et al. (1998) identified the EWR of OH ($1.6892\mu\text{m}$) and Mg ($1.5760\mu\text{m}$) as a diagnostic of T_{eff} . They also used the EWR of CO ($1.6207\mu\text{m} + 1.6617\mu\text{m}$) and Mg ($1.5760\mu\text{m}$) as a luminosity indicator (which reflects the surface gravity). Doppmann & Jaffe (2003) derived the T_{eff} , radial velocity, and the amount of veiling by fitting observational $2.2\mu\text{m}$ spectra with synthesized spectra. They estimated $\log g$ by calculating the EWR of the Na interval at $2.2\mu\text{m}$ (including the absorption lines of Na, Sc, Si) and the CO bandhead at $2.3\mu\text{m}$. When the EWR is calculated by taking the ratio of absorption lines separated, a correction for the amount of veiling is necessary, as it is wavelength dependent.

To derive the EWR directly from observed spectra without any veiling correction, we calculate EWRs using closely spaced absorption lines. This is practicable because the effects of veiling are nearly constant over small wavelength ranges. We present a new method for determining the age of mid- to late-K type PMS stars using EWRs of nearby absorption lines obtained from high-resolution I -band spectroscopy. We observed 30 giant stars, 6 main-sequence stars, and 4 weak-line T Tauri stars (WTTSSs) with T_{eff} of around 4200K to derive a relationship between $\log g$ and the EWRs of Fe (8186.7\AA , 8204.9\AA) and Na (8183.3\AA , 8194.8\AA).

2. Method

To make highly accurate determinations of PMS star age, precise $\log g$ estimation is necessary. We selected the wavelength range in I -band (8180\AA to 8210\AA), where strong atomic lines exist. This wavelength is suitable for low-mass PMS stars of which T_{eff} is around 4000K. Such PMS stars in the Hayashi phase (Hayashi 1961) evolve with roughly constant T_{eff} . Therefore, their age may be approximately determined from $\log g$.

The absorption lines used in the EWR must be selected with care to minimize uncertainty

in the resultant $\log g$ value. We selected the *I*-band Na lines (8183.3Å, 8194.8Å) and Fe lines (8186.7Å (blended with vanadium), 8204.9Å). These lines are sensitive to both T_{eff} and $\log g$. Na lines are one of the strongest lines in the *I*-band. They are reached to the limiting depth, and the wing of these absorption lines is pressure-broadened in stars with large g . Fe lines are also strong lines in the *I*-band, but they are not reached to the limiting depth. The Fe line strength decreases with increasing g , depending on the growth of continuum opacity. Therefore, EWRs calculated from Na and Fe absorption line pair (Fe/Na) are considered suitable for deriving stellar surface gravities. In addition, assuming the abundance ratios of the elements are equal, EWR has no dependence on metal abundance.

However, the relation between Fe/Na and surface gravity is yet unknown. To derive this relationship, a high-resolution spectroscopic observation of stars with fixed T_{eff} and varying $\log g$ was necessary. Since the surface gravities of PMS stars are between that of giants and main-sequence stars, we observed giants, main-sequence stars. Also the WTTSs were observed to verify the effectiveness of this method to PMS stars.

3. Observations and Data Reduction

3.1. Object Properties

The selected sample objects and their properties are listed in table 1. We selected 30 giants (including subgiants) and 6 main-sequence stars to estimate the relationship between g and the Fe/Na. All targets are single stars. 25 giants and 4 main-sequence stars have T_{eff} of 4200-4300K, since the radiation peak of these stars is in the *I*-band and they are bright enough to observe. Five giants and two dwarfs with T_{eff} of 4600-4700K were included to provide an estimate of the dependence of EWRs on T_{eff} .

To derive the surface gravity in advance, giants and main-sequence stars of which parallax was measured by the Hipparcos satellite (Perryman et al. 1997) were selected. The $\log g$ of these objects was calculated as follows:

$$\log g = \log \frac{M}{M_{\odot}} + 4 \log \frac{T}{T_{\odot}} - \log \frac{L}{L_{\odot}} + \log g_{\odot}, \quad (1)$$

where M is the mass, T the effective temperature, and L the luminosity. The luminosity was calculated from the *V*-band magnitude given in SIMBAD (taken from previous photometric studies), and the parallax. For the effective temperature, the T_{eff} -spectral type relationship (Lang 1992) was used. The error of the effective temperature is not included in the $\log g$ estimation and therefore the error of the $\log g$ may be underestimated. The relationship of M and spectral type in Drilling & Landolt (2000) was used to derive the masses of the main-sequence stars. The giant star masses were estimated by comparing luminosities and temperatures with the evolutionary tracks given in Lejeune & Schaerer (2001) (figure 1). Since giants smaller than $2.0 M_{\odot}$ evolve rapidly after the helium flash, we used the pre-flash evolutionary track for these

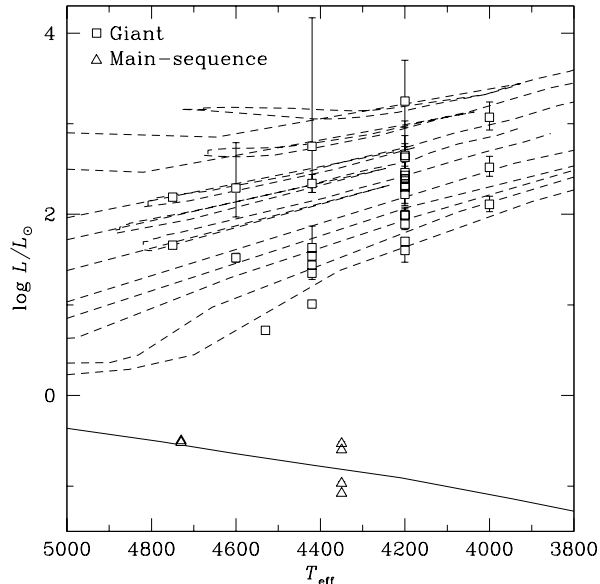


Fig. 1. The H-R diagram for the giants and main-sequence stars. The dashed lines are the evolutionary tracks from Lejeune & Schaerer (2001); $M = 0.90, 1.00, 1.25, 1.50, 1.70, 2.00, 2.50, 3.00, 4.00,$ and $5.00 M_{\odot}$ from the bottom. The solid line indicates the isochrone for 10^9 yr (Baraffe et al. 1998).

stars. The derived $\log g$ of β Gem (2.73 ± 0.01) is consistent with the result of a spectroscopic study (Drake and Smith 1991), in which it was estimated as 2.75 ± 0.15 . The large error in the surface gravity of the giants is attributable to the errors in luminosity (figure 1), which arise from the parallax errors.

Four WTTSs belonging to the Taurus-Auriga star-forming region were also added to our samples to test the effectiveness of the derived EWR- $\log g$ relationship. The $\log g$ of these WTTSs were also estimated from equation (1). Temperatures were estimated using Lang (1992), following the procedure for the main-sequence stars. We derived luminosities from photometry, including corrections for extinction (A_V), since the excess from the circumstellar disk is small. The A_V for HBC 374 and V827 Tau were taken from Kenyon & Hartmann (1995). For the other objects, RX J0452.5+1730 and RX J0459.7+1430, we estimated the A_V by fitting the SED corrected by an arbitrary A_V to the $V, J, H,$ and K -band magnitudes. The V -band magnitude was taken from SIMBAD, and the 2MASS catalog was used for the $J, H,$ and K -band magnitudes. The estimated A_V was 0.69 and 0.67 for RX J0452.5+1730 and RX J0459.7+1430, respectively. The mass of each star was estimated by using the H-R diagram, comparing the temperature and luminosity with the evolutionary model of Baraffe et al. (1998). The mass of HBC 374 and V827 Tau were $0.8 M_{\odot}$. On the other hand, the masses of RX J0452.5+1730 and RX J0459.7+1430 were $1.20 M_{\odot}$ and $1.25 M_{\odot}$, respectively. The distance to the Taurus-Auriga molecular cloud was fixed at 142 ± 14 pc (Wichmann et al. 1998).

3.2. Observations

High-resolution *I*-band spectroscopy of 30 giants and 6 main-sequence stars was carried out on 2007 January 17 to 24 and 2008 March 24 to 27 using the High Dispersion Echelle Spectrograph (HIDES) on the Okayama Astrophysical Observatory 1.88 m telescope. The slit width was set to $220\mu\text{m}$, giving a resolution of ~ 60000 . The angle of the red cross-disperser was selected to center the 69th order of the echelle spectrograph ($8165\sim 8300\text{\AA}$) on the 2048×4096 CCD. The integration time range was $90\sim 7200$ sec, yielding a S/N of ~ 100 . The maximum integration time was set to 1800 sec to reduce the risk of cosmic rays. Exposures of faint objects were divided into several frames. Flat frame were taken using the flat lamp equipped in the instrument, and were obtained at the beginning and end of each night's observations. Bias frames and Th-Ar lamp frames for wavelength calibration were taken with the same frequency.

The spectra of the 4 WTTSs were obtained using the Subaru Telescope with High Dispersion Spectrograph (HDS) on 2007 September 18. The slit width was set to $0.6''$ ($R\sim 60000$). The instrument was set to the StdNIRb mode, to obtain the Na and Fe absorption lines in the 73rd order. The integration time for each object was 900 sec. Flat, bias, and Th-Ar frames were also obtained.

3.3. Data Reduction

The data were reduced using Image Reduction and Analysis Facility (IRAF) software package¹. The same procedures were applied to both HIDES data and HDS data. First, the bias was removed for each frame by subtracting the average level of the overscan area of each frame, and also by subtracting the averaged bias frame. Flat fielding was accomplished with the normalized flat frame. Cosmic rays and scattered light were removed. Next, the spectrum was extracted from each object frame. The comparison data obtained with the Th-Ar lamp were used for wavelength calibration. When the object was taken several times, the spectra were combined after wavelength calibration to improve the signal-to-noise ratio. The spectra were normalized at the continuum level in the last procedure. Spectra samples are displayed in figure 2.

The SPLOT task was used to measure the equivalent width (EW) of each line, and the line was fit with the Voigt function. Since telluric lines appear in this wavelength range, we de-blended these lines from the photospheric lines. The EWs of some Na and Fe lines were difficult to measure because of heavy telluric line blending. The error in EW was estimated from uncertainty of the continuum level. The measured EWs of each object are listed in table 2.

¹ IRAF is distributed by the National Optical Astronomy Observatory.

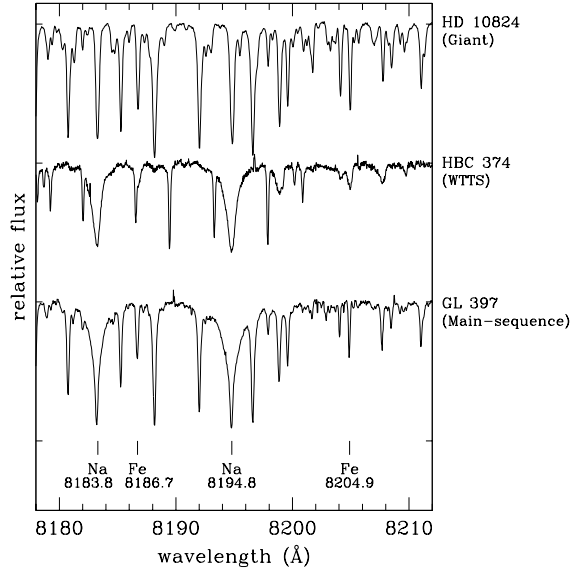


Fig. 2. Sample spectra of a giant, a WTTS, and a main-sequence star. The Doppler shift of each object is corrected. The absorption lines used to derive the EWRs are marked. Other sharp lines are mostly telluric lines. The Na (8183.3Å) and Fe (8186.7Å) in the WTTS spectrum are blended with the telluric lines.

4. Results and Discussion

4.1. Relationship between EWR and Surface Gravity

We derived a relationship between $\log g$ and the EWR of Fe and Na absorption lines (Fe/Na) for 25 giants and the 4 main-sequence stars of which T_{eff} are around 4200-4300K. We calculated the EWR using four line pairs: Fe (8186.7Å) / Na (8183.3Å), Fe (8186.7Å) / Na (8194.8Å), Fe (8204.9Å) / Na (8183.3Å), and Fe (8204.9Å) / Na (8194.8Å). Results are shown in figure 3. Filled squares and triangles mark the EWRs of the giants and main-sequence stars, respectively. The solid line in each graph is the best-fit line for these objects. In every case, the line ratios decrease significantly with increasing $\log g$. The averaged slope of the curves in $\log g = 3.5-4.0$ (a typical surface gravity for PMS stars) are -0.085, -0.067, -0.084, -0.064 in Fe (8186.7Å) / Na (8183.3Å), Fe (8186.7Å) / Na (8194.8Å), Fe (8204.9Å) / Na (8183.3Å), and Fe (8204.9Å) / Na (8194.8Å), respectively. These EWRs are considered to be an excellent diagnostics for deriving the surface gravity.

Next, we calculated the EWRs of five giants and two main-sequence stars of which T_{eff} is 4600-4700K. The EWRs of these objects are shown as open squares and triangles in figure 3. The best-fit line in each EWR is indicated as a dashed line. The EWRs increase for higher- T_{eff} objects at constant gravity over the range of $\log g = 3.5-4.0$. A comparison of fitted curves indicates that the EWRs of high- T_{eff} objects are 0.007-0.032 larger than the low- T_{eff} EWRs in $\log g = 3.5$.

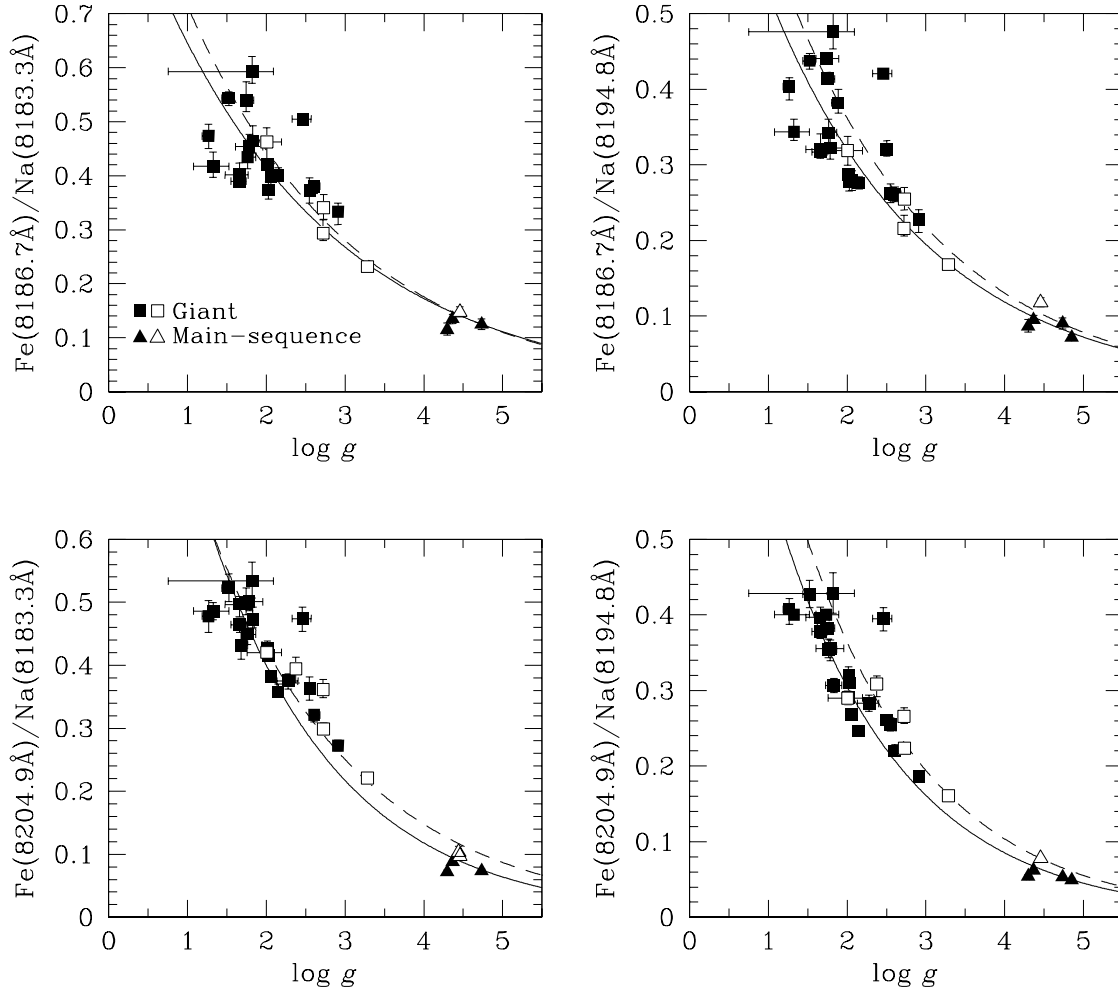


Fig. 3. EWR versus $\log g$ (g : cm/s^2). The squares mark the EWRs for the giants. The triangles mark the EWRs for main-sequence stars. The filled plots denote the EWRs of objects with T_{eff} around 4200-4300K, and the open plots are for 4600-4700K objects. The solid lines are the fitted curve for the 4200-4300K objects. The lines for the 4600-4700K objects are shown as dashed.

4.2. Model Atmospheric Spectra Comparisons

We synthesized spectra using the SPTOOL program (Takeda 1995), which calculates model spectra based on the ATLAS 9 model (Kurucz 1993). The model spectra were calculated for T_{eff} of 4200K and 4750K, and a range in $\log g$ of 1.0-5.0, and the EWRs were estimated (figure 4). All of the EWRs calculated from the synthesized spectra decreased with increasing $\log g$. This is consistent with the EWRs for the observed spectra.

In addition, although the EWRs of the observed spectra and the data from the SPTOOL are poorly matched especially in the EWRs from the 4750K model spectra and the Fe (8204.9Å) ratios, the EWRs of the high- T_{eff} objects are larger than those of low- T_{eff} objects with a $\log g$ range larger than 3. This occurs because the EW of the Fe lines increases, and the wing of the Na lines decreases in high- T_{eff} spectra.

This discrepancy in observed spectra and model spectra could arise from improper values of the excitation potential and the damping constant of the Fe and Na lines. Since the both observed and synthetic EWRs match in the Fe (8186.7Å) / Na (8183.3Å) and Fe (8186.7Å) / Na (8194.8Å) EWRs, the excitation potential and the damping constant of Fe (8186.7Å) line and both Na lines are seem to be estimated correctly. In the Fe (8204.9Å) case, since the observed EWs were weaker than the modeled EWs and has no strong wings, the excitation potential may be underestimated. Further improvements on the line data will increase the utility of this $\log g$ diagnostic.

4.3. The EWR of WTTS

We next compared the EWRs of WTTSs with the EWRs of giants and main-sequence stars. Since the Na (8183.3Å) and Fe (8186.7Å) lines of the WTTSs were blended with the telluric lines, only the Fe(8204.9Å) / Na (8194.8Å) was obtained.

As seen in figure 5, the EWRs of two WTTSs (RX J0452.5+1730 and RX J0459.7+1430, marked with open circles) with $T_{\text{eff}}=4590\text{K}$ are larger than the EWR of the WTTS (HBC 374, marked with filled circle) of which T_{eff} is 4060K. This is consistent with results from the fitted curves and the model spectra mentioned in section 4.2. The EWRs of high- T_{eff} WTTSs agree closely with the curve from the 4600-4700K objects, and the EWRs of HBC 374 and V827 Tau fits the curve approximated by the 4200-4300K objects. This result indicates that the surface gravity of PMS stars is able to be determined from this relationship.

By using this relationship, the $\log g$ of these two WTTSs are estimated at 3.95, which correspond to the age of 2.8 Myr in the evolution model of Baraffe et al. (1998). This result agrees with the age derived from the photometric observation using the extinction amount of Kenyon & Hartmann (1995) (table 3). However, using the amount of extinction of Furlan et al. (2006) results the $\log g$ of HBC 374 and V827 Tau to 3.263 and 3.627, respectively. The ages of these two WTTSs estimated by using this A_V will be less than 1 Myr, which mismatch our result.

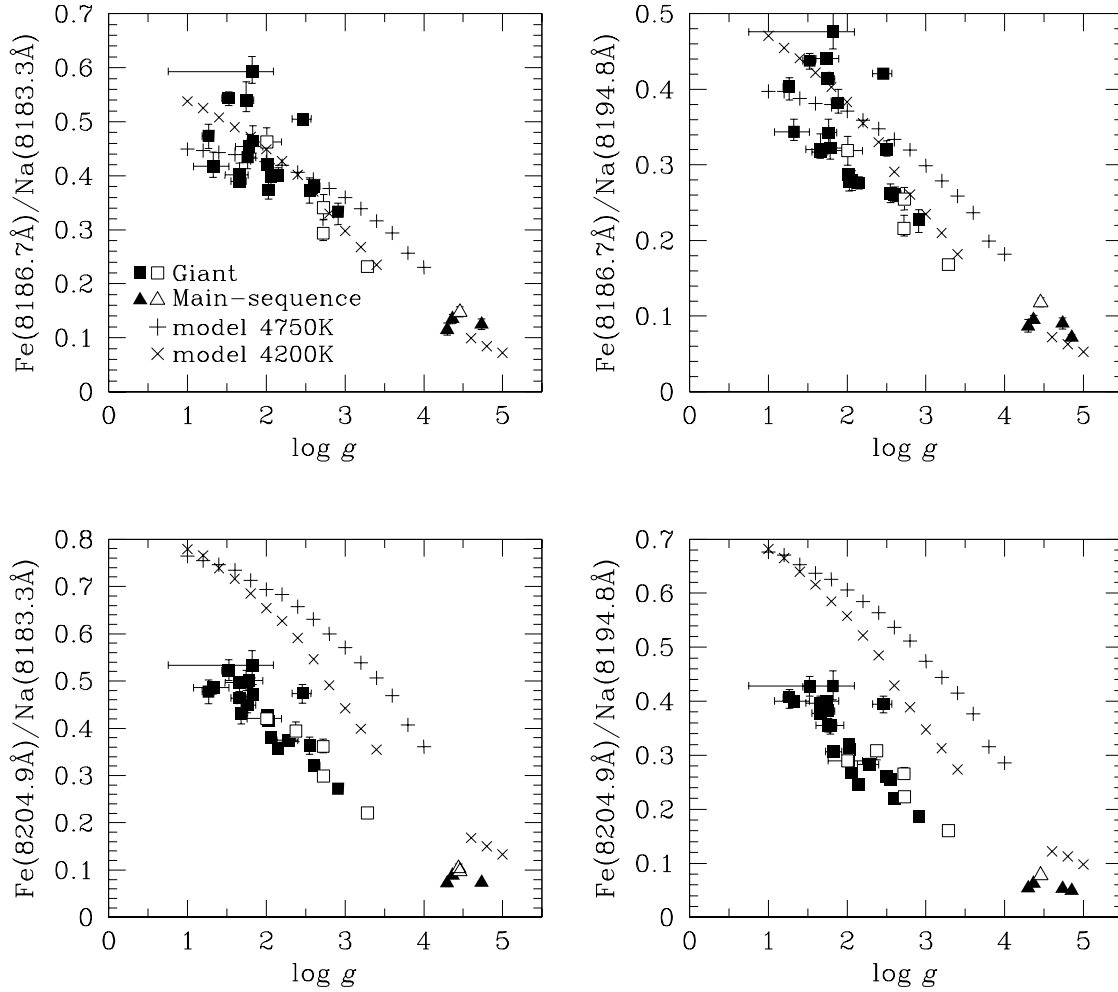


Fig. 4. EWR versus $\log g$ (g : cm/s^2) with the EWR of the model spectra created by SPTOOL. The squares indicate the EWR of the giants, and the triangles represent the main-sequence stars. The filled plots denote the EWRs of the 4200-4300K objects, and the open plots are for 4600-4700K objects. The plus and cross signs are the EWR from model spectra of $T_{\text{eff}} = 4750\text{K}$ and $T_{\text{eff}} = 4250\text{K}$, respectively.

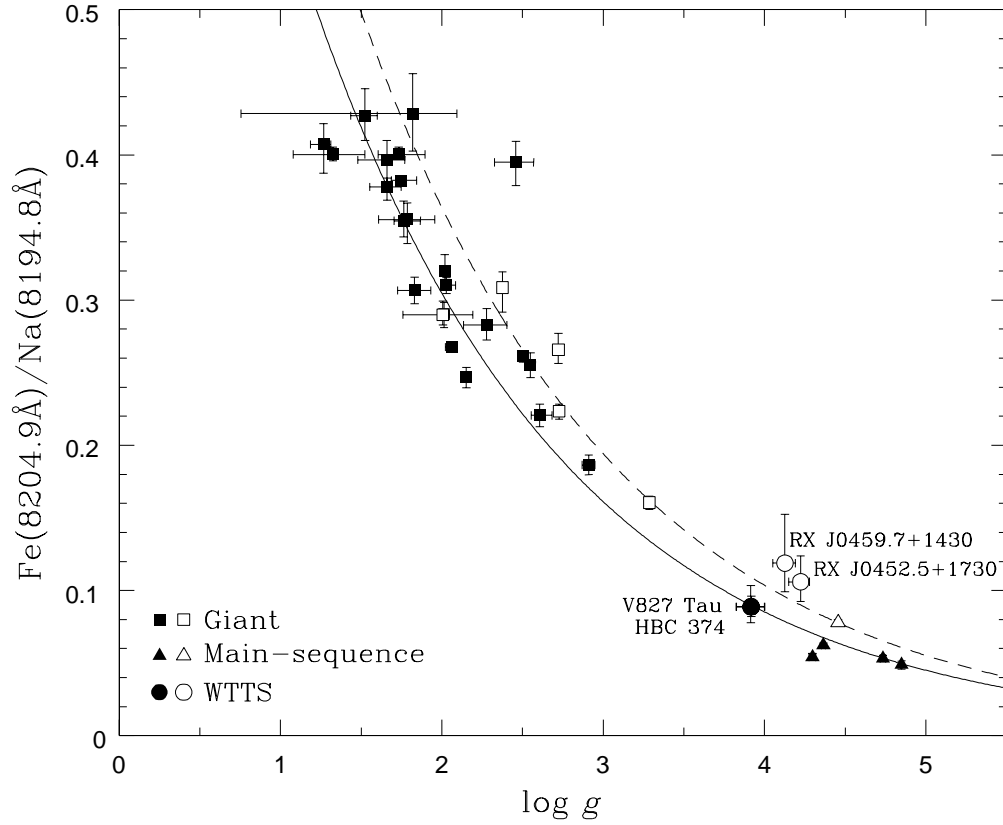


Fig. 5. EWR ($\text{Fe}(8204.9\text{\AA}) / \text{Na}(8194.8\text{\AA})$) versus $\log g$ ($g: \text{cm}/s^2$) for the EWR of WTTSs. The squares, triangles, and the fitted curves are from figure 3. The open and filled circles indicate the EWRs of WTTS of which $T_{\text{eff}} = 4590\text{K}$ and $T_{\text{eff}} = 4060\text{K}$, respectively.

4.4. Age Determination Accuracy

The age of a PMS star is able to be estimated by comparing the derived surface gravity with an evolution model (Baraffe et al. 1998; Siess et al. 2000). In our method, the accuracy of the calculated ages depends on the precision of the surface gravity value obtained for the PMS stars. This is dependent on the error in the EWR. We assumed the EWR error of the PMS star as 7.0×10^{-3} , which nearly corresponds to the error of HBC 374. The $\log g$ error calculated from this uncertainty is 0.1-0.2 in the 3.5-4.0 range. Consequently, by comparing with an evolution model of a $0.8 M_{\odot}$ star in Baraffe et al. (1998), the age of the PMS star can be determined within a factor of 1.5, in average. This precision will be improved by deriving the general EWR error in the other three EWRs. To adapt this method to PMS stars of different temperatures, accurate estimations of the relation of EWR- $\log g$ relationship for each T_{eff} range are required. In addition, an independent T_{eff} estimation is necessary in order to determine the $\log g$ of the pre-main sequence star using this technique.

5. Conclusion

We carried out high-resolution optical spectroscopy to create a new age determination method for late-K type PMS stars. To obtain a surface gravity indicator from the spectrum, we derived the EWR using nearby absorption lines, which avoid problems from veiling contamination and distance uncertainty.

The EW of the Na (8183.3Å and 8194.8Å) and Fe (8186.7Å and 8204.9Å) absorption lines in the *I*-band was used in this work. To derive the relationship between Fe/Na and surface gravity, we observed 25 giant stars, 4 main sequence stars, and WTTSs with the Okayama Astrophysical Observatory 1.88 m telescope and HIDES, and the Subaru Telescope and HDS. The T_{eff} of the objects were 4200-4300K and the surface gravity was known from the previous photometric studies. All four EWRs decreased with increasing surface gravity. Therefore, they are efficient diagnostics of surface gravity. Using the Fe (8204.9Å) / Na (8194.8Å) EWR, the $\log g$ of PMS stars with $0.8 M_{\odot}$ can be estimated with an uncertainty of 0.1-0.2. From comparisons with an evolution model, we concluded that their ages can be determined within a factor of 1.5.

Five giants, two main sequence stars, and two WTTSs with higher- T_{eff} (4600-4700K) were also observed to estimate the temperature dependence of the EWR. The EWRs of the high- T_{eff} objects were larger than those of the low T_{eff} in the typical PMS star surface gravity range. Therefore, to accurately determine the ages of PMS stars with masses larger or smaller than $0.8 M_{\odot}$, new EWR- $\log g$ relationship for each T_{eff} range are required. A precise estimation of EWR- $\log g$ relationship allow us to determine the accurate age of PMS stars and to study the evolution process of star and circumstellar materials.

We are grateful for the assistance given by the staff of the Okayama Astrophysical Observatory during the observations. We also thank the staff of the Subaru Telescope for the service observation.

References

- Baraffe, I., Chabrier, G., Allard, F. & Hauschildt, P. H. 1998, *A&A*, 337, 403
Cohen, M. & Kuhn, L. V. 1979, *ApJS*, 41, 743
Drake, J. J. & Smith, G. 1991, *MNRAS*, 250, 89
Doppmann, G. W. & Jaffe, D.T. 2003, *AJ*, 126, 3030
Drilling, J. S. & Landolt, A. U. 2000, in *Allen's Astrophysical Quantities*, ed. A. N. Cox (New York: Springer-Verlag), 389
Furlan, E., et al. 2006, *ApJS*, 165, 568
Kenyon, S. J. & Hartmann, L. 1995, *ApJS*, 101, 117
Hayashi, C. 1961, *PASJ*, 13, 450
Kurucz, R. L. 1993, *Kurucz CD-ROM*, No.13 (Cambridge: Smithsonian Astrophysical Observatory)
Lang, K. R. 1992, *Astrophysical Data: Planets and Stars* (New York: Springer-Verlag), ch. 9
Lejeune, T. & Schaerer, D. 2001, *A&A*, 366, 538
Meyer, M. R., Edwards, S., Hinkle, K. H., & Strom, S. E. 1998, *ApJ*, 508, 397
Palla, F. & Stahler, S. W. 2002, *ApJ*, 581, 1194
Perryman, M. A. C., et al. 1997, *A&A*, 323, L49
Siess, L., Dufour, E. & Forestini, M. 2000, *A&A*, 358, 593
Strom, K. M., Strom, S. E., Edwards, S., Cabrit, S. & Skrutskie, M. F. 1989, *AJ*, 97, 1451
Takeda, Y. 1995, *PASJ*, 47, 287
Wichmann, R., Bastian, U., Krautter, J., Jankovics, I. & Ruciński, S. M. 1998, *MNRAS*, 301, L39

Table 1. The list of the observed stars and their properties.

Name	Sp. Type	T_{eff} (K)	$\log g$ ($g: \text{cm s}^{-2}$)	S/N
Giants				
β Gem	K0IIIb	4750	2.73 ± 0.01	160
HD 19656	K0III	4750	2.38 ± 0.02	100
HD 76291	K1IV	4600	$2.72^{+0.02}_{-0.04}$	170
HD 100204	K1IV	4600	$2.01^{+0.19}_{-0.25}$	140
HD 145148	K1.5IV	4530	3.23 ± 0.03	170
HD 45512	K2III-IV	4420	2.55 ± 0.03	130
HD 101978	K2IV	4420	$1.82^{+0.27}_{-1.07}$	160
HD 106102	K2III-IV	4420	$2.61^{+0.08}_{-0.05}$	140
HD 108299	K2IV	4420	$2.46^{+0.11}_{-0.13}$	100
HD 110501	K2III-IV	4420	2.91 ± 0.04	110
HD 121146	K2IV	4420	2.50 ± 0.02	190
HD 147142	K2IV	4420	$2.03^{+0.06}_{-0.03}$	110
HD 49738	K3III	4200	$1.33^{+0.20}_{-0.25}$	110
HD 65759	K3III	4200	$1.66^{+0.09}_{-0.11}$	110
HD 86369	K3III	4200	$1.89^{+0.06}_{-0.09}$	160
HD 88231	K3III	4200	$1.76^{+0.10}_{-0.06}$	80
HD 102328	K3III	4200	2.15 ± 0.02	90
HD 109012	K3III-IV	4200	$2.28^{+0.12}_{-0.14}$	160
HD 113637	K3III	4200	$1.66^{+0.11}_{-0.18}$	120
HD 115478	K3III	4200	2.01 ± 0.03	140
HD 118839	K3III	4200	1.83 ± 0.10	130
HD 129245	K3III	4200	$2.02^{+0.03}_{-0.02}$	90
HD 132304	K3III	4200	$1.73^{+0.16}_{-0.13}$	130
HD 137688	K3III	4200	$1.79^{+0.17}_{-0.18}$	120
HD 146388	K3III	4200	$2.06^{+0.01}_{-0.04}$	140
HD 156093	K3III	4200	$1.75^{+0.10}_{-0.06}$	170
HD 163547	K3III	4200	$1.83^{+0.05}_{-0.06}$	190
HD 10824	K4III	4000	$1.52^{+0.08}_{-0.09}$	150
HD 20644	K4III	4000	$1.27^{+0.04}_{-0.08}$	100
HD 23413	K4III	4000	$1.68^{+0.08}_{-0.00}$	120
Main-sequence stars				
GL 105	K3V	4730	4.46 ± 0.01	270
GL 183	K3V	4730	4.44 ± 0.01	110
GL 141	K5V	4350	4.37 ± 0.01	120

Table 1. (Continued.)

Name	Sp. Type	T_{eff} (K)	$\log g$ (g : cm s $^{-2}$)	S/N
GL 380	K5V	4350	4.85 ± 0.00	220
GL 397	K5	4350	4.73 ± 0.02	130
GJ 3678	K5V	4350	4.30 ± 0.02	150
WTTS				
RX J0452.5+1730	K4	4590	$4.22^{+0.05}_{-0.07}$	60
RX J0459.7+1430	K4	4590	$4.13^{+0.07}_{-0.08}$	60
HBC 374	K7	4060	$3.92^{+0.08}_{-0.09}$	70
V827 Tau	K7	4060	$3.92^{+0.08}_{-0.10}$	70

Table 2. The list of the measured EW for each object.

Name	EW (\AA)			
	Na (8183.3 \AA)	Fe (8186.7 \AA)	Na (8194.8 \AA)	Fe (8204.9 \AA)
Giants				
β Gem	$0.280^{+0.009}_{-0.011}$	0.100 ± 0.006	$0.374^{+0.008}_{-0.009}$	0.084 ± 0.001
HD 19656	$0.264^{+0.014}_{-0.010}$	—	$0.337^{+0.016}_{-0.007}$	0.104 ± 0.003
HD 76291	0.251 ± 0.006	$0.074^{+0.007}_{-0.003}$	0.342 ± 0.008	$0.091^{+0.003}_{-0.002}$
HD 100204	$0.247^{+0.007}_{-0.005}$	$0.114^{+0.007}_{-0.008}$	$0.359^{+0.007}_{-0.009}$	0.104 ± 0.002
HD 145148	$0.313^{+0.006}_{-0.005}$	0.072 ± 0.001	0.431 ± 0.006	0.069 ± 0.002
HD 45512	$0.304^{+0.014}_{-0.011}$	$0.113^{+0.006}_{-0.005}$	0.434 ± 0.008	0.111 ± 0.003
HD 101978	$0.279^{+0.006}_{-0.008}$	$0.165^{+0.006}_{-0.005}$	$0.347^{+0.012}_{-0.013}$	0.149 ± 0.008
HD 106102	$0.341^{+0.011}_{-0.006}$	$0.130^{+0.001}_{-0.003}$	$0.496^{+0.017}_{-0.019}$	$0.109^{+0.001}_{-0.002}$
HD 108299	$0.274^{+0.007}_{-0.006}$	0.138 ± 0.001	$0.329^{+0.007}_{-0.006}$	$0.130^{+0.004}_{-0.005}$
HD 110501	0.315 ± 0.006	$0.105^{+0.005}_{-0.009}$	$0.460^{+0.013}_{-0.012}$	0.086 ± 0.002
HD 121146	—	$0.126^{+0.006}_{-0.005}$	$0.393^{+0.002}_{-0.001}$	$0.103^{+0.001}_{-0.002}$
HD 147142	$0.293^{+0.006}_{-0.005}$	0.109 ± 0.005	0.393 ± 0.008	$0.122^{+0.000}_{-0.001}$
HD 49738	0.309 ± 0.011	$0.129^{+0.007}_{-0.005}$	$0.375^{+0.004}_{-0.005}$	0.150 ± 0.001
HD 65759	$0.293^{+0.009}_{-0.008}$	0.114 ± 0.001	$0.360^{+0.010}_{-0.007}$	$0.136^{+0.000}_{-0.001}$
HD 86369	—	$0.145^{+0.006}_{-0.005}$	$0.381^{+0.007}_{-0.008}$	—
HD 88231	0.291 ± 0.013	0.126 ± 0.004	$0.368^{+0.014}_{-0.015}$	0.131 ± 0.001
HD 102328	$0.374^{+0.005}_{-0.012}$	0.150 ± 0.003	0.542 ± 0.012	$0.134^{+0.002}_{-0.003}$
HD 109012	0.289 ± 0.006	—	$0.383^{+0.010}_{-0.012}$	0.108 ± 0.003
HD 113637	$0.286^{+0.003}_{-0.002}$	$0.115^{+0.008}_{-0.004}$	$0.358^{+0.004}_{-0.007}$	$0.142^{+0.004}_{-0.006}$
HD 115478	$0.294^{+0.002}_{-0.001}$	$0.124^{+0.003}_{-0.002}$	$0.432^{+0.004}_{-0.002}$	$0.125^{+0.004}_{-0.005}$
HD 118839	—	—	$0.377^{+0.009}_{-0.010}$	0.112 ± 0.002
HD 129245	—	—	0.398 ± 0.006	0.127 ± 0.004
HD 132304	—	0.132 ± 0.002	$0.300^{+0.003}_{-0.004}$	0.120 ± 0.003
HD 137688	$0.248^{+0.002}_{-0.003}$	$0.113^{+0.007}_{-0.003}$	$0.350^{+0.013}_{-0.010}$	$0.124^{+0.002}_{-0.004}$
HD 146388	$0.277^{+0.004}_{-0.005}$	0.110 ± 0.007	0.394 ± 0.001	0.106 ± 0.001
HD 156093	$0.263^{+0.012}_{-0.016}$	$0.142^{+0.003}_{-0.002}$	0.343 ± 0.001	0.131 ± 0.001
HD 163547	$0.264^{+0.006}_{-0.008}$	$0.122^{+0.007}_{-0.005}$	—	$0.124^{+0.004}_{-0.002}$
HD 10824	$0.320^{+0.009}_{-0.008}$	$0.174^{+0.001}_{-0.002}$	0.398 ± 0.011	$0.167^{+0.006}_{-0.005}$
HD 20644	$0.347^{+0.016}_{-0.014}$	0.164 ± 0.004	$0.407^{+0.016}_{-0.007}$	0.166 ± 0.005
HD 23413	$0.322^{+0.010}_{-0.006}$	—	—	$0.139^{+0.009}_{-0.006}$
Main-sequence stars				
GL 105	$0.478^{+0.013}_{-0.014}$	$0.070^{+0.005}_{-0.004}$	0.596 ± 0.004	0.046 ± 0.001
GL 183	$0.629^{+0.008}_{-0.010}$	—	—	$0.065^{+0.007}_{-0.006}$

Table 2. (Continued.)

Name	EW (\AA)			
	Na (8183.3 \AA)	Fe (8186.7 \AA)	Na (8194.8 \AA)	Fe (8204.9 \AA)
GL 141	$0.826^{+0.031}_{-0.015}$	$0.111^{+0.007}_{-0.006}$	$1.171^{+0.020}_{-0.023}$	$0.073^{+0.001}_{-0.002}$
GL 380	—	$0.097^{+0.003}_{-0.004}$	$1.345^{+0.048}_{-0.052}$	$0.066^{+0.004}_{-0.002}$
GL 397	$0.940^{+0.017}_{-0.015}$	0.117 ± 0.011	$1.297^{+0.035}_{-0.028}$	0.069 ± 0.002
GJ 3678	$0.506^{+0.009}_{-0.007}$	$0.058^{+0.008}_{-0.006}$	$0.671^{+0.012}_{-0.006}$	$0.036^{+0.002}_{-0.001}$
WTTs				
RX J0452.5+1730	—	—	$0.772^{+0.026}_{-0.033}$	$0.082^{+0.015}_{-0.013}$
RX J0459.7+1430	—	—	$0.720^{+0.033}_{-0.065}$	$0.086^{+0.024}_{-0.017}$
HBC 374	—	—	$0.963^{+0.037}_{-0.026}$	0.085 ± 0.007
V827 Tau	—	—	$1.223^{+0.021}_{-0.053}$	$0.109^{+0.020}_{-0.017}$

The lines heavily blended with telluric lines were unmeasured (expressed "—").

Table 3. The age of the WTTs estimated from EWR and photometric method.

Name	Method				
	EWR	Photometric			
		KH95*		F06†	
Age (Myr)	A_V	Age (Myr)	A_V	Age (Myr)	
HBC 374	2.8	0.76	2.5	2.40	<1.0
V827 Tau	2.8	0.28	2.5	1.00	<1.0

* Kenyon & Hartmann (1995)

† Furlan et al. (2006)